Published in final edited form as:
Nanotechnology. 2010 February 26; 21(8): 85102. doi:10.1088/0957-4484/21/8/085102.

Tunable plasmonic nanobubbles for cell theranostics

EY Lukianova-Hleb[1], **EY Hanna**[2], **JH Hafner**[3], and **DO Lapotko**[1,3]

DO Lapotko: dmitri.lapotko@rice.edu

[1] Laboratory for Laser Cytotechnologies, A V Lykov Heat and Mass Transfer Institute, 15 Brovka Street, Minsk, 220072, Belarus

[2] Department of Head and Neck Surgery, The University of Texas M D Anderson Cancer Center, 1515 Holcombe Boulevard, Houston, TX, 77030, USA

[3] Department of Physics and Astronomy, Rice University, 6100 Main Street, Houston, TX 77005, USA

Abstract

Combining diagnostic and therapeutic processes into one (theranostics) and improving their selectivity to the cellular level may offer significant benefits in various research and disease systems and currently is not supported with efficient methods and agents. We have developed a novel method based on the gold nanoparticle-generated transient photothermal vapor nanobubbles, that we refer to as plasmonic nanobubbles (PNB). After delivery and clusterization of the gold nanoparticles (NP) to the target cells the intracellular PNBs were optically generated and controlled through the laser fluence. The PNB action was tuned in individual living cells from non-invasive high-sensitive imaging at lower fluence to disruption of the cellular membrane at higher fluence. We have achieved non-invasive 50-fold amplification of the optical scattering amplitude with the PNBs (relative to that of NPs), selective mechanical and fast damage to specific cells with bigger PNBs, and optical guidance of the damage through the damage-specific signals of the bubbles. Thus the PNBs acted as tunable theranostic agents at the cellular level and in one process that have supported diagnosis, therapy and guidance of the therapy.

1. Introduction

Combining diagnosis and therapy in one process is an emerging biomedical method referred to as theranostics [1,2]. A distinct goal of theranostics is to selectively target specific (diseased) tissues or cells to increase diagnostic and therapeutic accuracy. The major promise of theranostics is to bring together key stages of a medical treatment, such as the diagnosis and therapy, and thus to make a treatment shorter, safer and more efficient. However, this goal requires adequate tools with a high multi-functionality and selectivity. The initial phase of the development of theranostics has already revealed the two general challenges: lack of multi-functional methods and agents, and the lack of selectivity and specificity of available agents (that ultimately requires cell and molecular levels). Several theranostic methods have employed nanoparticles (NPs) as the carriers of diagnostic agents and drugs [3–5]. However, NPs themselves may also act as multi-functional agents due to their unique properties, such as the plasmon resonances of noble metal NPs, and without chemical loads. Plasmon resonances can be activated optically and convert incident light into scattered (optical) and absorbed (thermal) components with the potential for diagnostic and therapeutic applications.

So far plasmon resonant NPs have demonstrated excellent biocompatibility [6], optical diagnostic [7–10] and therapeutic potentials [7,9,11,12]. However, background scattering by cells and tissues often dominates the scattering signal, resulting in the low sensitivity of NP-

based imaging and diagnostic methods. This was improved with photothermal (PT) techniques [13], but required higher laser-induced temperatures that can be thermally detrimental to cells and molecules. Furthermore, the therapeutic applications of plasmon resonant NPs also employ PT effects such as hypothermia [7,9,12] and pressure waves [14] for inactivation of molecular and cellular targets. However, these are macro-rather than nanoscale effects that cannot be localized and precisely controlled within a single cell. All this, together with the challenges of NP delivery, poses significant limitations to combining accurate diagnosis and targeted therapy in a single and fast nanometer-scale process.

We hypothesized that a combination of the photothermal properties of plasmonic nanoparticles with those of the transient vapor bubbles may be a key solution of the above problems through the development of a tunable nanoscale theranostic probe that is not a nanoparticle but a nanoparticle-generated event—the plasmonic nanobubble (PNB), which combines high optical brightness with localized mechanical impact. In the current work we have studied the optical generation and detection of PNBs around gold nanoparticles in individual living cells, with the focus on tuning the PNB properties in one cell and evaluating the multi-functionality of the PNB.

2. Materials and methods

2.1. Principle of PNB theranostics

Cell theranostics employs a tunable and transient probe, and a vapor bubble (figure 1) is generated with a short laser pulse around plasmon resonant gold nanoparticles (NP), which we refer to as a plasmonic nanobubble. The PNB is a system that results from the interaction of optical radiation with a NP and its environment.

The optical and mechanical properties of PNB depend upon its diameter (tunable in the range of from 50 nm to 50 μm) and lifetime (tunable in the range of from 10 ns to 10 μs). The short lifetime of PNBs makes them highly transient phenomena that exist on demand. For target-specific generation of the PNBs we have selectively formed clusters of relatively safe gold NPs around molecular targets in cancer cells. Gold NPs, conjugated to diagnosis-specific antibodies have been delivered and aggregated into NP clusters through the mechanisms of antibody–antigen interaction and endocytosis (figure 1(a)). Remote (optical) and non-invasive activation and sensing of PNBs around such intracellular clusters was realized in individual living cells with free laser beams.

When activated by a laser pulse, an intracellular plasmonic nanoparticle (figure 1(b)) acts a heat source and generates a transient PNB in the surrounding medium. PNBs of nanometer-scale size and nanosecond-scale duration act as diagnostic probes by scattering light from the probe laser. Larger micrometer-scale PNBs provide a localized therapeutic action through a mechanical (non-thermal) impact due to their rapid expansion and collapse, thus disrupting the cell membrane(see figure 1(c)). Optical monitoring of the disruptive PNBs can guide their therapeutic action. Thus the PNBs may combine diagnostics, therapy, and therapy guidance. Despite the extensive studies of the photothermal properties of nanoparticles [7, 15, 16] the generation of photothermal vapor bubbles around them remains an under-recognized phenomenon. Although laser-induced macro-bubbles have been studied for various biomedical tasks [17], the studies of bubbles around optically excited nanoparticles [18] at the nanometer scale [19] are rather scarce. Furthermore, the PNBs differ appreciably from the macro-bubbles, where the threshold laser fluence for bubble generation increases with the size of the absorber [20]. For nanoparticles the reverse is true: the bigger the size of the plasmonic nanoparticles, the lower the laser fluence threshold for bubble generation [21–23]. In addition, PNBs concentrate the laser-induced thermal impact around the nanoparticles, unlike macro-bubbles [21, 22]. To improve the selectivity of the

PNB generation we have targeted cells with relatively small functionalized NPs (which can enter cells unlike larger absorbers) that formed intracellular NP clusters due to receptor-mediated endocytosis [24, 25]. At a set laser fluence, the nanoparticle cluster will generate a PNB, where individual nanoparticles will not due to their smaller size [21, 24, 25]. Thus, PNBs can be selectively generated in specific cells, do not use chemicals, and rely only on nanometer-scale phenomena of light and heat that are natural for all living systems.

2.2. Generation of PNBs

PNB generation was experimentally realized by using laser pulse-heated intracellular gold NPs. Evaporation of the medium around a nanoparticle (NP) involves several processes: laser pulse-induced thermalization of a NP occurs in 1 ps [16]; thermal diffusion from a NP to adjoining medium forms a thin vapor layer around a NP; finally, the PNB begins to expand to a maximal diameter and then collapses. The bubble lifetime may be considered as proportional to its maximal diameter [17,19,20,26,27]. The minimal fluence of a single laser pulse that provides bubble generation is defined as the PNB threshold fluence. PNBs were generated around 50 nm gold spheres and in individual living cells. The pulse wavelength (532 nm) and duration (0.5 ns) were chosen so to provide maximal localization of the released heat and at the same time to avoid the generation of shock and pressure waves. If the localization of a photothermal (PT) impact is required, there should be no pressure and shock waves, and also the thermal diffusion losses should be minimized. When the optical pulse duration exceeds the acoustic relaxation time, no pressure or shock wave would emerge. Next, when the optical pulse duration is less than the thermal relaxation time, the losses due to thermal diffusion are negligible, and the entire heat released is concentrated in a small volume around the heat source. In our work we have employed a pulse of length 0.5 ns, 532 nm (STA-01 SH, Standa Ltd, Vilnius). The pump laser beam was directed into the illumination path of an inverted optical microscope and was focused into the sample. Single cells or NPs and single events were studied (figure 2).

2.3. Detection and imaging of the PNBs

PNB detection has been realized with two optical methods that take advantage of the excellent optical scattering properties of bubbles [28]. These methods were applied earlier by us for the imaging of the photothermal phenomena in living cells with the pump–probe laser microscope that we have developed [29,30]. The time-resolved imaging of NPs and PNBs was realized by using side illumination of the sample with a custom made pulsed probe dye laser beam (0.5 ns) at a wavelength 690 nm and with a tunable time delay of 1–10 ns relative to the pump pulse (figure 2). The scattered by NP or by PNB probe radiation was imaged with the digital camera (Luka, Andor Technologies, Ireland). For quantitative analysis of the optical amplification by the PNB we have introduced the relative scattering amplitude $K_{sc}(t) = [I(t) - I_b]/[I(0) - I_b]$ that describes the pixel image amplitude $I(t)$ of optical scattering by a PNB relative to that by a NP, $I(0)$ (I_b is the average pixel image amplitude of the background). While allowing one to 'see' the PNB the pulsed imaging can hardly provide kinetic measurement. The latter was realized in a time response mode. An additional continuous probe beam (633 nm) was directed to the sample collinearly with the probe pulse and its axial intensity was monitored by a high-speed photodetector (PDB110AC, Thorlabs Inc.). The time response mode allowed measurement of the PNB lifetime that characterizes a maximal diameter of the bubble and thus allows one to quantify its therapeutic impact. Image and response modes were used simultaneously, thus combining the imaging and measuring of the lifetime (figure 2).

2.4. Cells

For the *in vitro* experimental model we have used gold spheres of 50 nm and their conjugates with anti-epidermal growth factor receptor (EGFR) antibody C225 that were

obtained from Nanopartz Inc (Salt Lake City, UT). The cells were prepared as the monolayers of living EGFR-positive lung carcinoma cells (A549) that were grown into standard 9 mm culture wells (#C24765, Molecular Probes, Inc., Eugene, OR). All cells were incubated with NPs for 30 min at 37 °C. The concentration of the NPs during the incubation was adjusted to 0.9×10^{11} ml^{-1}. NP-C225 conjugates were selectively coupled with EGFR. This provided a maximal relative concentration of NPs at the cellular membrane of cancer cells. Secondly, during receptor-mediated endocytosis the NPs were internalized and concentrated into clusters of closely packed NPs in endosomal compartments. At the end of the incubation procedure large NP clusters were formed only in those cells with high initial levels of membrane-bounded NPs, i.e. the target cells, as we have shown earlier [24,25].

Cell viability was evaluated optically with two standard microscopy techniques. First, a bright field image was obtained for the cell before and after its exposure to a single pump pulse and the difference of these two images was used to detect any PNB-induced changes of the shape of the cell, in particular, emerging of the blebbing bodies. Blebbing bodies may develop in the cells with damaged cytoskeleton and even with an intact membrane. Second, the membrane damage by the PNB was detected using a standard fluorescent method by monitoring the cellular uptake of ethidium bromide (EtBr) dye that enters only the cells with a compromised membrane. Fluorescent images were obtained for each cell before and after PNB generation. Though these methods did not provide monitoring of the long-term viability, they could be applied on site and to specific individual cells during the generation of the PNBs and without removing the cells from the sample chamber. Individual cells (60 in each population) were irradiated with single laser pulses at 532 nm, which is close to the peak of the maximum of the plasmon resonance of the gold NPs. The laser beam diameter was 14 μm in the sample plane to provide the exposure of the whole cell. Thus the single events were analyzed in individual cells. Each experiment was repeated from 3 to 5 times with a newly grown cell population.

3. Results

3.1. Gold NP-generated PNBs in living cells

Generation and detection of tunable PNBs in living cells was studied in individual living A549 lung carcinoma cells. The cells were targeted with conjugates of 50 nm gold spheres to anti-epidermal growth factor receptor antibody C225 and then were exposed *in vitro* to a single pump laser pulse at a wavelength near the nanoparticle plasmon resonance peak (0.5 ns, 532 nm). Optical scattering of the pulsed probe beam (690 nm) by the gold NPs and by the PNBs in the cells was measured as an image pixel amplitude (figure 3-II). Also, the lifetime of the PNB was measured as the duration of a PNB-specific time response that was simultaneously obtained (figure 3-III). We have monitored the damage to the individual cells after their exposure to the laser pulse by fluorescent imaging of the uptake of the ethidium bromide (that stains cells with a disrupted membrane) and the blebbing (that is associated with the cytoskeleton damage). Scattering by gold NPs accumulated by individual A549 cells after 30 min incubation at 37 °C (figure 3(a)-II) was found to be quite low and its image amplitudes were close to the scattering image amplitudes associated with cellular organelles. We have used the NP scattering image as a reference for quantifying the amplification of optical scattering by the PNBs. The first pump laser pulse was applied to individual cells at a fluence of 0.24 J cm^{-2} (above the bubble generation threshold), which induced a PNB within the cell, as was detected with the probe laser image (figure 3(b)-II). The lifetime of this PNB was relatively short, 25 ns, according to its time response (figure 3(b)-III). This PNB has amplified the scattering by 9.2 times relative to the scattering by the gold NPs. After the PNB generation bright field (figure 3(b)-IV) and fluorescent (figure 3(b)-V) microscopy images of the cell showed no deviation from the pre-pulse conditions shown in figure 3(a)-IV, V, respectively. The absence of fluorescence and blebbing implies

that the cell has survived the laser pulse and the PNB. We have detected only one PNB despite the apparent fact that endocytosis assumes the internalization of many NPs. This can be explained with the threshold nature of the PNB: the fluence level was sufficient for the generation of the PNB only around the biggest clusters of NPs, while this fluence was below the PNB generation threshold for the smaller NP clusters or single NPs. This result has demonstrated high specificity of the PNB generation compared to the specificity of the nanoparticle imaging (figure 3(a)-II). The sensitivity of PNB diagnosis versus NP diagnosis is clearly seen by comparing figure 3(a)-II with (b)-II: under identical imaging conditions the amplitude of the NP scattering was much lower than that for the PNB scattering so it did not produce any detectable image.

Next, the second laser pulse was shortly applied to the same cell at the increased fluence of 1.76 J cm^{-2}. The second PNB (figure 3(c)-II) was much brighter with its scattering amplitude being amplified 290 times relative to that of the NPs and was also much longer (figure 3(c)-III) than the 1st PNB. Within 30–60 s after the PNB generation the fluorescent image has shown the penetration of the dye inside the cell (figure 3(c)-V) and the bright field image has shown the formation of the blebbing bodies (figure 3(c)-IV). These have indicated the disruption of the cellular membrane and, possibly, of the cytoskeleton. This experiment has demonstrated the ability to tune the intracellular PNB by varying the laser fluence from non-invasive imaging (with an almost 10-fold improvement in optical scattering signal) to cell disruption.

3.2. PNB and cell damage

We have studied the cell-damaging properties of the PNBs by varying the laser pulse fluence so as to analyze the probability of bubble generation and the probability of cell damage among intact (untreated) and NP-treated cells. Each single cell in the population was irradiated with a single laser pulse of specific fluence and then the cell population-averaged values were obtained (figure 4(a)). NP treatment has lowered the threshold laser fluence for the bubble generation by almost 30 times relative to the intact cells (figure 4(a), table 1). As a function of pulse laser fluence, the probabilities of cell damage and of the bubble generation coincided for intact cells, but were significantly separated in the NP-treated cells (figure 4(a)). At pulse fluences of 0.06–0.22 J cm^{-2}, intracellular PNBs were generated in NP-treated cells without damaging the majority of the host cells (figure 4(a)), while the same cells were damaged at 10 times higher fluences (table 1).

We have simultaneously measured the lifetime of the PNB in each irradiated cell as a function of the laser pulse fluence. For relatively small PNBs their lifetime is nearly proportional to their maximal diameter [17,19,20,26,27] and was used as its measure. The PNB lifetime has increased linearly with the laser fluence in the NP-treated and in the intact cells (figure 4(b)). The lifetime of the non-invasive PNBs was found to be about 5 times shorter than that of the damaging ones (table 1). This implies a similar difference in the maximal diameters of non-invasive and damaging PNBs. We consider that the maximal diameter of the PNB plays the major role in the cell damage: small PNBs do not damage the cell, while the increase of the PNB size by several times has induced almost immediate disruption of the cellular membrane and skeleton, as was revealed with fluorescent (membrane damage—see figure 3(c)-V) and bright field (appearance of the blebbing bodies —see figure 3(c)-IV) microscopy. The assumption about the mechanical damage mechanism is in line with our recent data on the thermal insulating effect of PNBs [21,22] (that have proved that, unlike laser-heated NPs, PNBs do not deliver significant thermal impact to their environment) and with independent data for opto- and sonoporation of the cells [31–38]. The latter studies have used ultrasound and optical breakdown mechanisms to induce vapor (cavitation) bubbles at cell membranes and have reported that the vapor bubbles with the diameter above 2 μm caused irreparable damage to cellular membranes. Based on the

obtained results we have estimated the cell damage threshold lifetime of the PNB to be about 110 ns. We have found that intact cells cannot support such small non-lethal PNB (table 1) and the generation of the photothermal laser-induced bubbles was always associated with cell damage [39,40], suggesting that the endogenous optical absorbers in intact cells cannot generate small PNBs. As for the NP-treated cells, we may suggest that the PNBs with a maximal diameter smaller than 300 nm would be non-invasive to living cells (PNB function: non-invasive imaging), those in the range of 500–1000 nm would produce local reversible disruption (PNB function: intracellular delivery of the drugs or other agents), and PNBs in the range from 1 to 10 μm would mechanically destroy individual cells (PNB function: cell damage).

We have also found that at laser fluences below the PNB generation threshold, the NPs in cells still were significantly heated by the laser pulse but did not cause detectable damage to the cells. Also, the exposure of the cell to 16 pump laser pulses (at 15 Hz frequency), instead of a single pulse, did not influence the cell viability and the level of the damage threshold fluence, which suggests that the cell damage results from a single event rather than from an accumulative effect of the sequence of the PNBs. Thus, the PNB damage mechanism is mechanical, non-thermal, and rapid: a single laser pulse induces an expanding PNB that disrupts the cellular cytoskeleton and plasma membrane causing the blebbing and cell staining with the membrane-penetrating dye. Also, during the generation of the cell-damaging PNBs with sub-microsecond lifetime, we did not observe the damage in the collateral cells where no PNBs were generated. This has demonstrated a cell level selectivity of the PNB mechanism of cell damage. Our ongoing work will include the study of the cell structure after the PNB generation and of the long-term viability of the surviving cells (including a zebrafish *in vivo* model). Nevertheless, the NP-generated intracellular PNBs have demonstrated a localized, fast, selective and easily controllable (through the laser pulse fluence level) mechanism of cell damage.

The optical parameters of the damaging PNBs differ significantly from those of the non-invasive PNB: the lifetime was several times longer (table 1) and the image pixel amplitude was 10–50 times higher. This may allow direct and simultaneous guidance of the cell damage due to the PNB and without additional techniques. The detection of any intracellular PNB with the image amplitude and/or lifetime being above specific thresholds can be considered as a sign of cell damage since these PNB parameters have correlated to the damage-related phenomena observed independently with the standard methods.

3.3. PNBs as optical probes

Finally, we have evaluated the sensitivity and specificity of the PNBs as imaging probes. We have measured the optical scattering amplification effect of small (non-invasive) PNBs as a function of the PNB lifetime, since the lifetime correlates with the bubble diameter (see figure 4(c)). The data presented were averaged for the cell populations and were obtained at specific laser pulse fluences. The amplification coefficient K_{sc} (measured relative to scattering amplitudes for gold NPs) linearly increases with the PNB lifetime. This implies the PNB-based mechanism of the amplification: the vapor–liquid border of the PNB creates a gradient of the refractive index, and the scattering efficiency of the PNB is determined by its diameter (that correlates to the PNB lifetime). The PNBs have yielded 10–50-fold optical amplification without disrupting the cell membrane or inducing blebbing.

Our previously reported modeling of PNB optical scattering [28] has predicted such amplification. In this work we have used a Mie simulation code, developed for multilayer concentric spheres, to model the scattering by the vapor bubble (with gold NP inside) relative to the scattering by a gold NP alone. By applying the developed model for gold spheres and silica–gold shells of the various dimensions we have found the general trend of

increase in scattering against bubble radius. This can be qualitatively understood from Rayleigh scattering, which states that the scattering intensity is proportional to d^6/λ^4, where d is the particle diameter and λ is the wavelength, provided d is smaller than λ. Compared to NPs alone, PNBs could potentially produce 1–3 orders of magnitude amplification in scattering intensity. The modeling results obtained, as well as the above experimental results, predict the better scattering efficiency of the bubble compared to the NP, mainly due to the increased diameter of the bubble and to the vapor–liquid interface that it temporary creates. A probe of such large diameter (up to 200–500 nm) cannot be delivered into the cell without compromising its viability, though it can be temporally generated there for a short time and in non-invasive way. Furthermore, our model has predicted an optical attenuating effect around NPs that do not generate the bubbles but are also heated with the pump laser pulse above the evaporation threshold for the environment. This attenuating effect has recently been confirmed by us in experiments with gold NPs in water [23]. Therefore, applying the single pulse at a specific fluence we may selectively amplify, by several orders of magnitude, the optical scattering around clusters of gold NPs while suppressing the scattering around single NPs or small clusters. The amplification/attenuation effect can be optimized by adjusting the fluence of the pump pulse so as to provide maximal specificity of PNB diagnosis.

Specificity of the diagnosis and selectivity of the therapy are the top priorities in cancer treatment. These were the objectives for developing the NP cluster mechanism for the generation of plasmonic nanobubbles. The specificity of PNB diagnosis depends upon NP parameters as of the PNB sources and can be significantly increased if NP clusters, not single NPs, are used to generate the PNBs. This rule has been verified during our previous studies of PNBs [21,23–25]: the aggregation of NPs into a cluster significantly lowered the PNB generation threshold fluence of the pump laser pulse. Therefore, at a specific fluence level the PNBs will be generated only around NP clusters and will not emerge around single (e.g. non-specifically coupled) NPs. Thus we have considered intracellular NP clusterization as the main solution to improving diagnostic specificity and therapeutic selectivity of the PNBs. To prove this concept we have experimentally varied the parameters that influence NP clusterization through the mechanism of receptor-mediated endocytosis: diagnosis-associated vectors conjugated to gold NPs (EGFR antibodies versus non-conjugated NPs), targeting conditions and also have compared the PNB generation in aqueous suspensions of the same gold NPs and their clusters. We have varied several endocytosis-related parameters. We have decreased the incubation temperature to 4 °C (which suppresses endocytosis) and have used the NPs without a C225 antibody. In both cases PNB generation thresholds increased from 0.09 ± 0.03 to 0.11 ± 0.06 J cm^{-2} (for 4 °C incubation with NP-C225) and to 0.33 ± 0.18 J cm^2 (for 37 °C incubation with unconjugated NPs), which implies that NP-C225 conjugates were selectively linked to EGFR and then were internalized through the receptor-mediated endocytosis.

Next, we have independently verified the physical basis for the selectivity of the PNB generation around the NP clusters compared to single NPs. The PNBs were generated and detected in water suspensions around the single gold NPs (50 nm spheres) and around their clusters that were intentionally prepared by adding NaCl into the suspension of the NPs. NP clusterization was verified by monitoring the extinction spectra of the NP suspensions (showing one plasmon peak near 532 nm) and their clusters (showing significant broadening of the peak though still without shifting its maximum). We compared the PNB generation threshold fluences in living cells and around isolated NPs and their clusters. The intracellular PNB generation threshold fluence (0.09 ± 0.03 J cm^{-2}) was found to be closer to that for the NP clusters in water (0.055 ± 0.02 J cm^{-2}) rather than the threshold for the single NPs in water (0.18 ± 0.06 J cm^{-2}). This also indicates that the generation of the intracellular PNBs occurs around NP clusters and not around single NPs. Also, the

clusterization of the NPs has lowered the PNB generation threshold by almost three times. Therefore, no PNBs could have been generated around single NPs (including those non-specifically coupled to non-target cells) at the laser pulse fluence level that is sufficient for the generation of the PNBs around the NP clusters. These results illustrate the improved specificity and selectivity of the PNB method relative to those based on the direct application of NPs as optical or thermal agents: the specificity and selectivity of the NP-based methods (such as optical scattering diagnosis and hypothermia, see the Discussion for details) is compromised by the unavoidable contribution from non-specifically coupled (targeted) single NPs. In our method, a few non-specifically coupled NPs could not form a big cluster that requires a considerable amount of NPs accumulated at cell membrane. Therefore, the biggest clusters can be formed only in target cells, thus providing the basis for the cell-specific theranostic application of PNBs.

4. Discussion

The above experiments have demonstrated several interesting features of intracellular NP-generated PNBs:

- the PNB probe is a transient event, not an object and so its load and presence in the cell are minimized to sub-microsecond times, while it uses relatively safe gold nanoparticles and low levels of laser fluence in a single pulse mode;
- the main diagnostic and therapeutic property of the PNB is characterized by its maximal diameter (lifetime) that can be precisely controlled and varied in the sub-micrometer range with the fluence of the laser pulse; also the PNB diameter can be conveniently monitored through the PNB lifetime and scattering amplitude;
- as the PNB can concentrate, within its volume, the thermal energy released by the NP [21,22], its outer action has a mainly mechanical, non-thermal nature and this may prevent thermal damage to surrounding molecules and collateral normal cells.

It is interesting to compare the PNB with currently available multi-functional probes that have been reported for theranostic applications and that can be classified into several groups (table 2): fluorescent probes [41–44], capsule-type probes (liposomes, micelles, polyelectrolyte and polymer capsules) [45–51], non-plasmonic nanoparticles [1,42–44,52,53], plasmonic nanoparticles [7,9,42,54] and gas-filled or cavitation bubbles [31–34,55,56]. Their theranostic properties were analyzed for the diagnosis, therapy and guidance, and also for cell level selectivity and safety (table 2). As for the fluorescent probes, the PNB may provide the ultimate imaging sensitivity: it was reported previously that the optical scattering efficiency of gold nanoparticles is 4–5 orders of magnitude higher than the fluorescent efficiency of the brightest fluorescent molecules [57], and we have demonstrated in our experiments that the optical scattering efficiency of PNB is 10–100 times higher than that for gold nanoparticles. Therefore, we may conclude that PNBs will provide much better imaging sensitivity than fluorescent probes. The specificity demonstrated for PNB cannot be achieved through nanoparticle scattering (or through fluorescence) because any non-specifically coupled NP (or fluorescent probe) increases the optical background and the probability of false-positive diagnosis. The combination of improved brightness of the PNBs with the threshold mechanism of their generation around NP clusters (that can be selectively formed around target molecules and cells as we have shown previously in [25,58]) principally improves the specificity of PNB diagnosis relative to NP- or fluorescent probe-based methods.

The other example is related to therapeutic properties of plasmonic NPs that are optically heated with continuous [7,9] or pulsed [11,12] optical radiation. The thermal mechanism of cell death was associated with doses of laser energy in the range from 30 to 1000 J cm^{-2},

while the PNB mechanical mechanism required doses within 1 J cm^{-2} (figure 4(a)). Also we have observed rather fast cell death with the direct signs of mechanical disruption of cellular components, and this did not depend upon apoptosis or necrosis as in the case of photothermal- or chemotherapies.

As for theranostics, despite widespread efforts, none of the current methods or probes (table 2) have been able to support imaging, delivery, therapy and guidance in one process, or with one probe and at the cell level. This task requires tuning the property and function of the probe in real-time and assumes: (1) the intracellular amplification of the optical signal, (2) the efficient delivery of the molecular loads and imaging probes to their intracellular targets, and selective inactivation (damage, elimination) of specific cells without collateral damage, (3) localized therapeutic action and (4) optical guidance of the delivery and therapy. As we have suggested above, a tunable transient nanoscale PNB as a theranostic probe can match all of the above requirements. First, PNBs may support several processes: sensing (diagnosis), delivery, therapy and optical guidance of the delivery and therapy (table 2). Second, PNBs may provide the cell level selectivity and specificity. Third, being transient phenomena, PNBs use safe gold nanoparticles with excellent targeting properties but are on-demand phenomena that do not exist until activated with an optical pulse. Fourth, unlike larger macrobubbles, PNBs can be generated in a controllable way to provide imaging and delivery functions in individual cells.

These advantages of the PNBs result from the tunable nature of optical and mechanical properties that are determined by the size of the bubble. This parameter can be precisely controlled through the optical pulse. Furthermore, the optical scattering efficiency of the bubble directly correlates to its diameter and so can be used to guide a biological action that is determined by its diameter: delivery of endocytosed molecules by intracellular PNB that disrupt the endosomes (smallest bubbles); delivery of the extracellular molecules through the perforation of the cellular plasma membrane (PNBs with increased diameter), controlled release of an encapsulated molecular load (by disrupting the capsule such as liposome), direct therapeutic action through mechanical irreversible disruption of cellular components and elimination of specific individual cells (cell-size bubbles), and microsurgical action with the largest bubbles that mechanically eliminate micro-tissue with an accuracy of 20–50 μm. The selectivity and specificity of PNBs basically depend upon the efficiency of targeting of gold NPs, but can be significantly improved (relative to other nanoparticle methods) due to NP clustering and the threshold nature of the bubble generation (as has been demonstrated during our preliminary studies).

The heterogeneous nature of clusterization of NPs can make the bubble diameter and generation threshold fluences less predictable. NP cluster formation is a physiological process that is difficult to control by physical methods, and this may create a certain challenge for PNB-based methods. However, we have shown that the NP cluster formation can also be controlled through such parameters as the time and temperature of cell incubation, NP concentration and conjugation to diagnosis-specific antibodies. Furthermore, the pump fluence can be adjusted to a level that provides one PNB per cell, as was shown in figure 3(b) (around the largest cluster). This implies an additional advantage of PNB over other agents, whose efficacy and sensitivity depend upon the total amount of molecules or nanoparticles delivered into the cell, while the PNB methods require a much lower (100–1000 times) number of nanoparticles to form at least one big cluster.

PNB generation and detection *in vivo* critically depend upon the delivery and control of light in heterogeneous tissues. The general solution is to provide a temporary optically transparent medium at the local site of the PNB generation (figure 5). One optical fiber probe can be used for the injection of NPs (figure 5(a)), an optically transparent medium (figure 5(b)), for

delivery (figure 5(b)) and collection (figure 5(c)) of optical radiation. We may consider three types of PNB applications: extracorporeal methods for processing liquid tissues; surface scanning methods for processing superficial or subcutaneous tumors (figure 5); delivering the NPs in a transparent buffer and light with a single probe (catheter, needle) into deep tissues. An important advantage of the PNB for *in vivo* applications is its stealth nature: the PNB does not exist in a tissue unless locally generated by a laser pulse. However, this work will require future *in vivo* and clinical testing. Recently we have suggested and tested an interesting solution for *in vivo* evaluation of PNB theranostics by using optically transparent zebrafish instead of 'classical' animal models such as rats and mice. PNBs were non-invasively generated and detected in zebrafish embryos and all of them have survived the PNBs. Also, the therapeutic potential of PNBs has been evaluated by us with clinical samples of the bone marrow of patients diagnosed with acute lymphoblast leukemia [24]. We have achieved 99–100% level of damage to the leukemia cells, while only 17% of normal cells have been damaged. This study has involved only therapeutic application of PNBs and cannot be considered as clinical testing of PNB theranostics, although it has demonstrated the clinical potential of PNBs.

5. Conclusions

The obtained results are the first and laboratory stage proof of the principle for theranostics with plasmonic nanobubbles. In the future PNBs can provide a universal platform for basic biomedical research, diagnosis and therapy. Several potential applications of PNBs include (1) high-sensitivity non-invasive imaging (based on amplified optical scattering), (2) controlled release, transfection and intracellular delivery (based on localized disruption with the PNBs of specific capsules, endosomes and cellular membrane), and (3) selective and guided cell and tissue damage. Our method was realized with a standard optical microscope. Due to the brief duration of the PNB (nanosecond range) our method can also be realized in flow cytometry and in microfluidic devices. The stealth nature of the PNB, which is not present in the sample until being remotely activated, and the safety of gold NPs may provide for their *in vivo* applications. Finally, a real-time tunability of the PNB optical and mechanical properties may allow the combination of different processes in one fast sequence of PNB-supported operations: detecting the target with a small non-invasive PNB, destroying the target with a bigger PNB by applying a second laser pulse of increased fluence, and monitoring the destruction though the optical properties of the destructive PNB. Such a theranostic method can be accomplished within a microsecond timescale and can also be extended to molecular or tissue targets. The experimental results presented here have demonstrated proof of the principle for the PNB theranostic method in individual living cells:

- the ability to use an on-demand activated agent—plasmonic nanobubble—for diagnostic and therapeutic purposes by tuning its maximal diameter and by using its optical and mechanical properties;
- non-invasive amplification (50-fold relative to the scattering by NPs) of optical scattering by the PNBs in specific cells;
- damage-specific optical parameters of the PNBs (lifetime and optical image amplitude) in the disruptive mode provide the basis for the real-time guidance of PNB therapy at the cellular level.

The development of a universal nontoxic theranostic probe with tunable properties may provide rapid translation of new technologies into the clinical phase. Although aimed at cancer, our methods are universal and can be applied to other pathological conditions since the plasmonic nanobubbles can be used at the molecular, cellular and tissue levels.

Acknowledgments

The authors acknowledge the support from NIH grant 1R21CA133641 and from the Institute of International Education/SRF.

References

1. Hooper JW. Med Lab Obs. 2006; 38:22.
2. Picard FJ, Bergeron MG. Drug Discov Today. 2009; 7:1092. [PubMed: 12546841]
3. Chanda N, Shukla R, Katti KV, Kannan R. Nano Lett. 2009; 9:1798. [PubMed: 19351145]
4. Daou TJ, Li L, Reiss P, Josserand V, Texier I. Langmuir. 2009; 25:3040. [PubMed: 19437711]
5. Rosi NL, Giljohann DA, Shad Thaxton C, Lytton-Jean AKR, Min SH, Mirkin CA. Science. 2006; 312:1027. [PubMed: 16709779]
6. Lewinski N, Colvin V, Drezek R. Small. 2008; 4:26. [PubMed: 18165959]
7. Huang X, El-Sayed I, Qian W, El-Sayed M. J Am Chem Soc. 2006; 128:2115. [PubMed: 16464114]
8. Kumar S, Harrison N, Richards-Kortum R, Sokolov K. Nano Lett. 2007; 7:1338. [PubMed: 17439187]
9. Loo C, Lowery A, Halas N, West J, Drezek R. Nano Lett. 2005; 5:709. [PubMed: 15826113]
10. Walter NG, Huang C-Y, Manzo AJ, Sobhy MA. Nat Meth. 2008; 5:475.
11. Pitsillides M, Joe EK, Wei X, Anderson RR, Lin CP. Biophys J. 2003; 84:4023. [PubMed: 12770906]
12. Tong L, Zhao Y, Huff TB, Hansen MN, Wei A, Cheng J-X. Adv Mater. 2007; 19:3136. [PubMed: 19020672]
13. Boyer D, Tamarat P, Maali A, Lounis B, Orrit M. Science. 2002; 297:1160. [PubMed: 12183624]
14. Lee S, Anderson T, Zhang H, Flotte TJ, Doukas AG. Ultrasound Med Biol. 1996; 22:1285. [PubMed: 9123654]
15. Govorov O, Richardson H. Nano Today. 2007; 1:30.
16. Hartland G. Phys Chem Chem Phys. 2004; 6:5263.
17. Hutson S, Ma X. Phys Rev. 2007; 99:158104.
18. Kotaidis V, Dahmen C, von Plessen G, Springer F, Plech A. J Chem Phys. 2006; 124:184702. [PubMed: 16709126]
19. Vogel A, Linz N, Freidank S, Paltauf G. Phys Rev Lett. 2008; 100:038102. [PubMed: 18233040]
20. Hüttmann G, Birngruber R. IEEEJ Sel Top Quantum Electron. 1999; 5:954.
21. Lapotko D. Opt Express. 2009; 17:2538. [PubMed: 19219157]
22. Lapotko D. Int J Heat Mass Transfer. 2009; 52:1540.
23. Lapotko D, Lukianova-Hleb E. Nano Lett. 2009; 9:2160. [PubMed: 19374436]
24. Lapotko D, Lukianova E, Potapnev M, Aleinikova O, Oraevsky A. Cancer Lett. 2006; 239:36. [PubMed: 16202512]
25. Lapotko D, Lukianova-Hleb E, Oraevsky A. Nanomedicine. 2007; 2:241. [PubMed: 17716124]
26. Brennen, CE. Cavitation and Bubble Dynamics. New York: Oxford University Press; 1995.
27. Ohl C-D, Kurz T, Geisler R, Lindau O, Lauterborn W. Phil Trans R Soc A. 1999; 357:269.
28. Marston, PL. Light scattering by bubbles in liquids and its applications to physical acoustics. In: Crim, LA.; Mason, TJ.; Reisse, JL.; Suslick, KS., editors. Sonochemistry and Sonoluminescence. Dordrecht: Kluwer Academic; 1999. p. 73-86.
29. Lapotko D, Kuchinsky G, Potapnev M, Pechkovsky D. Cytometry. 1996; 24:198. [PubMed: 8800552]
30. Hleb EY, Ying Hu, Drezek RA, Hafner JH, Lapotko DO. Nanomedicine. 2008; 3:797. [PubMed: 19025454]
31. Liu HL, Chen WS, Chen JS, Shih TC, Chen Y, Lin WL. Ultrasound Med Biol. 2006; 32:759. [PubMed: 16677935]
32. McDannold NJ, Vykhodtseva NI, Hynynen K. Radiology. 2006; 241:95. [PubMed: 16990673]
33. Guzmán HR, Nguyen DX, Khan S, Prausnitz MR. J Accoust Soc Am. 2001; 110:588.

34. Guzmán HR, Nguyen DX, Khan S, Prausnitz MR. J Accoust Soc Am. 2001; 110:597.
35. Ohl CD, Wolfrum B. Biochim Biophys Acta. 2003; 1624:131. [PubMed: 14642823]
36. Postema M, van Wamel A, Lancee CT, de Jong N. Ultrasound Med Biol. 2004; 30:827. [PubMed: 15219962]
37. Vogel A, Noack J, Hüttmann G, Paltauf G. J Phys: Conf Ser. 2007; 59:249.
38. Neumann J, Brinkmann R. J Biomed Opt. 2005; 10:024001. [PubMed: 15910075]
39. Lapotko D. Lasers Surg Med. 2006; 38:240. [PubMed: 16470847]
40. Lapotko D, Lukianova K. Int J Heat Mass Transfer. 2005; 48:227.
41. de Jong M, Breeman WA, Kwekkeboom DJ, Valkema R, Krenning EP. Acc Chem Res. 2009; 42:873. [PubMed: 19445476]
42. Ma D, Jakubek ZJ, Simard B. J Nanosci Nanotechnol. 2006; 6:3677. [PubMed: 17256315]
43. McCarthy JR, Jaffer FA, Weissleder R. Small. 2006; 2:983. [PubMed: 17193154]
44. Bryson JM, Fichter KM, Chu W-J, Lee J-H, Li J, McLendon PM, Madsen LA, Reineke TM. Proc Natl Acad Sci USA. 2009; 106:16913. [PubMed: 19805101]
45. Al-Jamal WT, Al-Jamal KT, Tian B, Cakebread A, Halket JM, Kostarelos K. Mol Pharmacol. 2009; 6:520.
46. Blanco E, Kessinger CW, Sumer BD, Gao J. Exp Biol Med. 2009; 234:123.
47. Schmieder AH, Caruthers SD, Zhang H, Williams TA, Robertson JD, Wickline SA, Lanza GM. FASEBJ. 2008; 22:4179.
48. Saad M, Garbuzenko OB, Ber E, Chandna P, Khandare JJ, Pozharov VP, Minko T. J Control Release. 2008; 130:107. [PubMed: 18582982]
49. Torchilin VP. AAPSJ. 2007; 9:E128. [PubMed: 17614355]
50. Khemtong C, Kessinger CW, Gao J. Chem Commun. 2009; 24:3497.
51. Sajja HK, East MP, Mao H, Wang YA, Nie S, Yang L. Curr Drug Discov Technol. 2009; 6:43–51. [PubMed: 19275541]
52. Santra S, Kaittanis C, Grimm J, Perez JM. Small. 2009; 5:1862. [PubMed: 19384879]
53. Pan D, Lanza GM, Wickline SA, Caruthers SD. Eur J Radiol. 2009; 70:274. [PubMed: 19268515]
54. Prigodich AE, Seferos DS, Massich MD, Giljohann DA, Lane BC, Mirkin CA. ACSNano. 2009; 3:2147.
55. Kennedy JE. Nat Rev Cancer. 2005; 5:321. [PubMed: 15776004]
56. Coussio CC, Farny CH, Haar GT, Roy RA. Int J Hypertherm. 2007; 23:105.
57. El-Sayed IH, Huang X, El-Sayed MA. Nano Lett. 2005; 5:829. [PubMed: 15884879]
58. Hleb E, Hafner J, Myers J, Hanna E, Rostro B, Zhdanok S, Lapotko D. Nanomedicine. 2008; 3:647. [PubMed: 18817468]

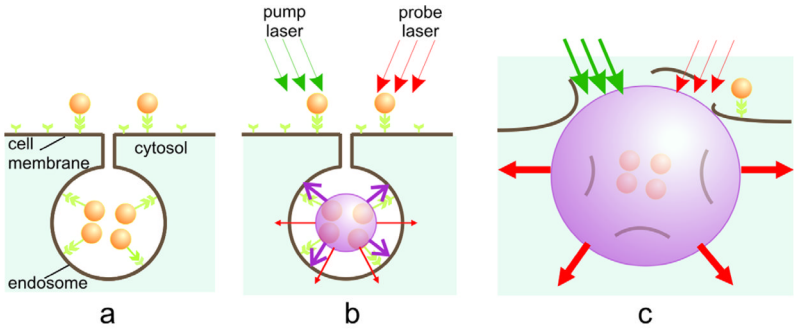

Figure 1.
PNB cell theranostic with multi-stage tunable PNB: (a) cell is targeted with NP-antibody conjugates and intracellular NP clusters are formed through the receptor-mediated endocytosis, (b) the 1st (diagnostic) PNB provides the data on a cell and allows one to determine the parameters of the next laser pulse, (c) the 2nd PNB delivers mechanical impact (cell damage though membrane disruption is shown) and this action is guided through the increased optical scattering (red arrows) of the 2nd PNB; the PNB is tuned by varying the fluence of the pump pulse (green arrows).

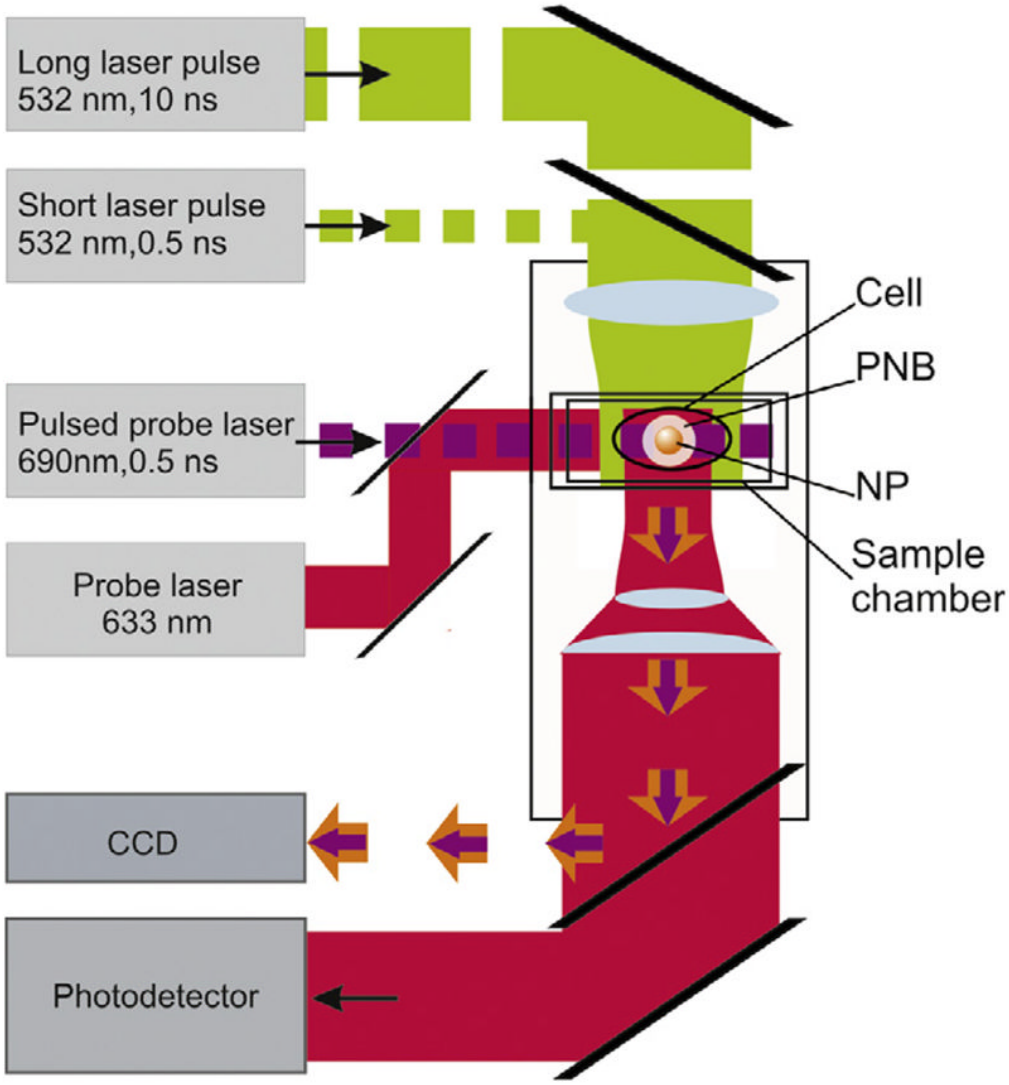

Figure 2.

Experimental setup: single gold NPs in water or individual cells in the sample chamber were mounted on the stage of an inverted optical microscope; PNB generation was provided by focused single pulses (532 nm, 0.5 ns); a pulsed probe laser (690 nm, 0.5 ns) provided time-resolved optical scattering imaging of the PNB and a continuous probe laser (633 nm, 1 mW) provided monitoring of the optical scattering of PNBs though their time responses. An additional pulsed laser (532 nm, 10 ns, 1 mJ cm^{-2}) was used for excitation of fluorescence in the cells.

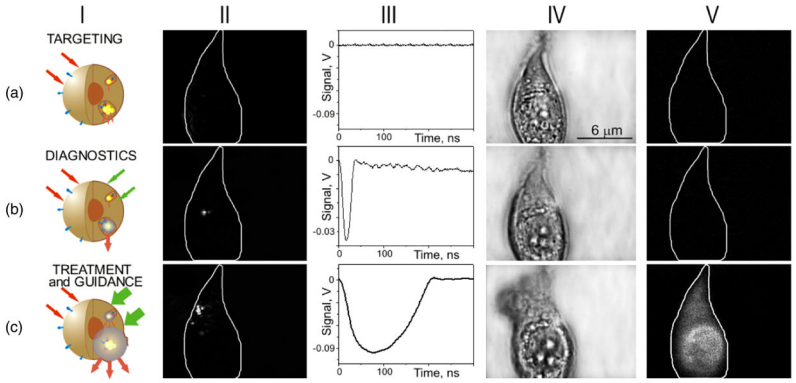

Figure 3.

Targeting the cell with gold NPs (a) and optical generation and detection of the intracellular PNBs: the 1st one non-invasively amplifies optical scattering (b), while increasing the fluence of the pump laser pulse induces the 2nd PNB that mechanically damages the cell (c); I—stages of the PNB theranostic action, II—optical pulsed scattering images of one cell with the membrane border shown with a white line, III—optical time response of the PNB shows its lifetime, IV—bright field and V—fluorescent (ethidium bromide-specific) images of the cell show it before (a) and after the generation of the 1st (b) and the 2nd (c) PNBs.

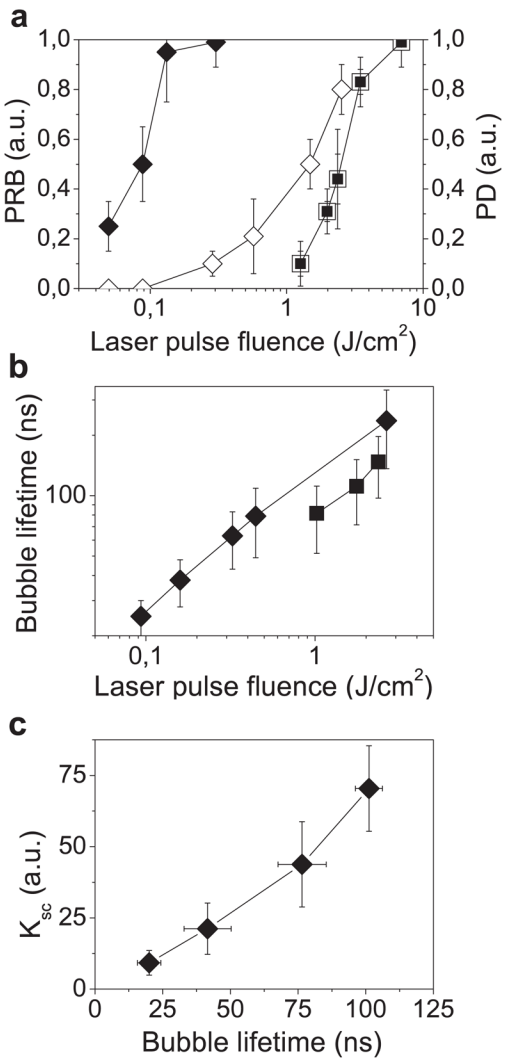

Figure 4.

Influence of the fluence of a single pump laser pulse (532 nm, 0.5 ns) on the PNB parameters and on the damage as measured in individual A549 cells: (a) PNB generation probability (PRB): (◆)—cells incubated with NP-C225 conjugates, (■)—intact cells; cell damage probability (PD): (◇)—cells incubated with NP-C225 conjugates, (□)—intact cells; (b) PNB lifetime: (◆)—cells incubated with NP-C225 conjugates, (■)—intact cells; (c) amplification of optical scattering amplitude by the PNB (relatively to gold NPs) in the NP-treated cells as function of the PNB lifetime (i.e. maximal size of the PNB).

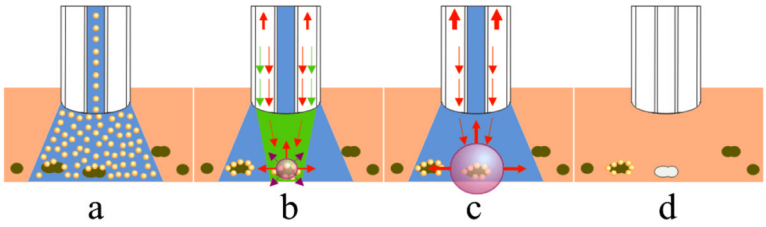

Figure 5.

Future clinical application scheme for PNB theranostics for treating superficial and subcutaneous tumors and metastases. (a) Injection of the buffer suspension of gold NP conjugates that selectively cauterize around cancer cells (dark green); (b) diagnosis stage: optically transparent buffers flush unbound NPs and create an optically transparent medium for irradiation of the targeted cancer cells with a short pump pulse (green) that selectively generates the PNB around the NP clusters; small nanobubbles act as optical scattering probes for the detection of cancer cells with the probe laser (red); (c) therapy: selective mechanical destruction of the cancer cells is provided by the 2nd, bigger PNB generated with the second pump laser pulse, and is optically guided though the destruction-specific scattering of the probe laser radiation by the 2nd PNB; (d) as a result of the 2-pulse process the cancer cells are selectively eliminated without damage to collateral normal cells.

Table 1

Parameters of the PNBs and intracellular photothermal bubbles.

Experimental parameters	Process and cell state	NP-treated cells (PNB)	Intact cells (cell chromophore-generated photothermal bubbles)
Pump laser (532 nm, 0.5 ns)	PNB generation	0.09 ± 0.03	2.72 ± 1.8
threshold fluence (J cm^2)	Cell damage	1.0 ± 0.75	2.72 ± 1.8
PNB lifetime (ns)	Surviving cells	44 ± 17	n/a
	Damaged cells	213 ± 100	145 ± 50

Table 2

Comparison of the diagnostic, therapeutic and guidance potentials of the common biomedical probes (high—very efficient, low—not efficient or not applied (or low selectivity, specificity)).

	Function				
Probe	**Diagnosis**	**Therapy**	**Guidance**	**Cell level selectivity and specificity**	**Safety**
Fluorescent probes	High	Low	High (drug conjugates)	High	Low (chemical toxicity)
Micelles, polymers and liposomes	Low (unless loaded with other probes)	Low	Low (unless loaded other probes)		depends upon release method
Nanoparticles (general)	High (magnetic resonance imaging)	High (thermal therapy)	Low	Low (magnetic resonance and photo-acoustic imaging)	Low (chemical toxicity)
Plasmonic nanoparticles	High (optical scattering and photo-acoustic imaging)	High (photo-thermal therapy)	Low	High (delivery and optical scattering imaging)	High for gold nanoparticles
Gas and cavitation bubbles	High (acoustic and optical imaging)	High	Low	Low	High